Evaluation and applications of shielding parameters for a heavy-ion accelerator facility

Noriaki Nakao[1,2], Hee-Seock Lee[1]
[1]Pohang Accelerator Laboratory (PAL), POSTECH, Nam-gu, Pohang, Republic of Korea
[2]Institute of Technology, Shimizu Corporation, Etchujima, Koto-ku, Tokyo, Japan

Abstract

For the conceptual design of shield for the Rare Isotope Science Project (RISP) in the Republic of Korea, the source term and attenuation length of shielding parameters for a simple exponential formula were determined by means of Monte Carlo simulations using the PHITS code. Simulations were performed for angular and energy spectra of secondary neutrons emitted from an iron target of full stopping thickness or from a thin graphite target bombarded by heavy ions of ^{238}U, ^{86}Kr, *or* ^{48}Ca *(200–270 MeV/u), or by protons (600 MeV) for the in-flight target system. A simulation with 70-MeV proton bombardment was also performed for the isotope separator on-line (ISOL) target system. The simulations of the transmission of high-energy neutrons through 8-m-thick shields of concrete or iron were performed using the neutron-energy spectra for various angles. By fitting the exponential formula to the attenuation profiles, shielding parameters were obtained for various combinations of projectile, target, angle, and shielding material. The parameters were summarised for a point beam loss and for uniform beam loss along the accelerator beam line. Appropriate thicknesses for concrete and iron shields in the heavy-ion accelerator facility can be estimated fairly easily for various conditions.*

Introduction

As part of the Rare Isotope Science Project (RISP) in the Republic of Korea, there are plans to use a heavy-ion beam of a few hundred kilowatts of power to achieve effective production of rare isotope (RI) beams using an in-flight target or an isotope separator on-line (ISOL) target system. For such a high-power accelerator facility, it will be necessary to construct a massive shielding wall, probably several meters thick, between the beam line and areas in which personnel work. Because neutrons readily penetrate the matter, the prompt radiation behind a shield consists mainly of neutrons among the secondary particles generated by beam losses at beam dumps, targets, or beam-line components.

Recently, Monte Carlo codes have been widely used to simulate beam interactions and radiation transport at accelerator facilities. However, the simulation of particle transmission with deep penetration through a massive shield generally requires sophisticated techniques and consumes large amounts of computing time. To avoid such complexities in the earlier stages of the conceptual design of the facility, empirical equations with an exponential form, such as the Moyer model [1], are frequently used to evaluate the external dose rate produced by prompt radiation through a massive shield. However, the parameters used in this model generally relate to proton accelerators with energies in excess of several gigaelectron volts [2] [3].

In this work, shielding parameters for heavy ions were investigated by means of a Monte Carlo simulation. Source terms and attenuation lengths for a simple exponential formula were estimated for various targets irradiated by heavy ions or protons with energies of several hundreds of megaelectron volts.

Empirical formula

Generally, the level of prompt radiation behind a massive shield can be expressed approximately by using a simple exponential formula. Images of applicable situations for a beam parallel to the shield and a beam perpendicular to the shield are shown in Figure 1.

For a point beam loss, the dose rate H [μSv/h] arising from prompt radiation at an estimation point can be expressed as follows:

$$H = JH_0 \frac{1}{r^2} \; exp\left(-\frac{d\rho}{\lambda}\right) \tag{1}$$

where J [W] is the beam injection at the source point, H_0 [(μSv/h) cm^2 /W] is the source term, r [cm] is the distance between the beam loss and the estimation points ($r = a + d$), a [cm] is the part of distance r in space, d [cm] is the part of distance r in the shield, ρ [g/cm^3] is the density of the shielding material, and λ [g/cm^2] is the attenuation length.

Figure 1: Images of applicable situations for point losses of parallel and perpendicular beams

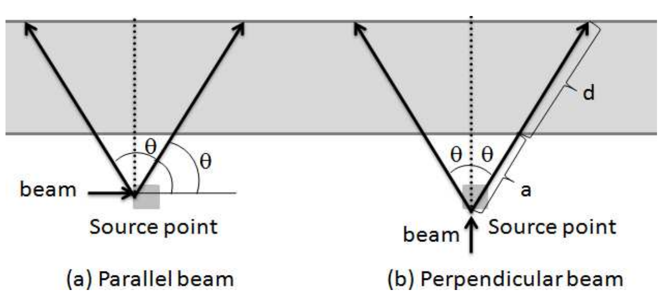

In the case of a multilayer shielding structure, the formula can be adjusted through multiplication by additional exponential parts for the extra materials, as follows:

$$H = JH_0 \frac{1}{r^2}\ exp\left(-\frac{d_1\rho_1}{\lambda_1}\right) exp\left(-\frac{d_2\rho_2}{\lambda_2}\right)\cdots \tag{2}$$

In the case of uniform beam loss along the beam line, the dose rate behind a massive shield can be expressed as follows:

$$H = \frac{dJ}{dL}\ H_0\ \frac{1}{r}\ exp\left(-\frac{d\rho}{\lambda}\right) \tag{3}$$

where dJ/dL [W/m] is the amount of uniform beam loss per unit length and H0 [(Sv/h) cm/(W/m)] is the source term. The other parameters in Equation (3) are the same as those in Equation (1). Equation (3) can be used only for the parallel beam, and the parameters r, d, and a are the distances in the direction perpendicular to the shield.

Monte Carlo simulation

For all Monte Carlo simulations in this work, we used the PHITS code [4] version 2.15. As data libraries for the simulation, we used JENDL-3.3 [5] nuclear data for low-energy neutrons below 20 MeV, and MCPLIB02 [6] for photon production and transportation.

Simulation of secondary neutron production

The characteristics of the targets used for the simulations are listed in Table 1. A thin graphite target of thickness 0.9 g/cm^2 was used as an in-flight target for the RI beam production. The target used in the simulation had a radius of 25 mm, a thickness of 4 mm, and a density of 2.25 g/cm^3. This target thickness is equivalent to a 5-mm-thick target with a density of 1.8 g/cm^3. Thick iron targets were chosen for the estimation of the source term for beam losses at beam-line components due to a beam halo or an operational failure. The thicknesses of these iron targets were chosen to be around 1.1–1.2 times thicker than the stopping range of projectiles, because the maximum flux of high-energy neutrons above 20 MeV is available in the forward direction when the thickness is in the projectile range for the case of heavy ions. The self-shielding effect of high-energy neutrons in the forward direction is not negligible for 600-MeV protons in the 30-cm-thick iron target. However, reducing the radius suppresses the self-shielding effect, not only in the sideways and backward directions, but also in the forward direction. The radius of the iron targets for all projectiles was chosen to be 5 mm, which is short enough to give a negligible neutron self-shielding effect in combination with negligible escape of the primary beam from the sides of the target.

An ISOL target is also used for the RI beam production from 70-MeV protons. As listed in Table 1, the target is of full stopping length and consists of a 3-cm-thick piece of UC_2 behind a 4-mm-thick graphite window and with a 5.4-mm-thick graphite dump.

The angular and energy spectra of the secondary neutrons produced from the target–projectile combinations listed in Table 1 were simulated in the energy range above 1 MeV. In the simulation, secondary neutron currents were estimated in the spherical surfaces of parts of the cone shapes for nine angular ranges. Angular and energy spectra of neutrons for various projectile injections for an in-flight target system are shown in Figures 2 and 3 for the iron and the graphite target, respectively. For an ISOL target system, the spectra from the iron and the ISOL targets irradiated by 70-MeV protons are shown in Figure 4.

Table 1: Characteristics of targets used in the simulations

	Iron (7.8 g/cm^3)			Graphite (2.25 g/cm^3)			
Projectile	Radius [mm]	Thickness [mm]	Range [mm]	Radius [mm]	Thickness [mm]	dE [MeV/u]	E-out [MeV/u]
200 MeV/u ^{238}U	5	2.0	1.7	25	4	167.6	32.4
240 MeV/u ^{86}Kr	5	5.0	4.5	25	4	52.0	188.0
270 MeV/u ^{48}Ca	5	10.0	9.6	25	4	25.9	244.1
600 MeV proton	5	300.0	279	25	4	2.1	597.9
70 MeV proton	5	9.0	7.8				
ISOL target (Graphite 1.8 g/cm^3, UC_2: 2.5 g/cm^3)							
70 MeV proton	R=35 mm	Graphite window (4 mm)+UC_2 (30 mm)+graphite dump (5.4 mm)					Full stop

Figure 2: Angular and energy spectra of secondary neutrons from an iron target

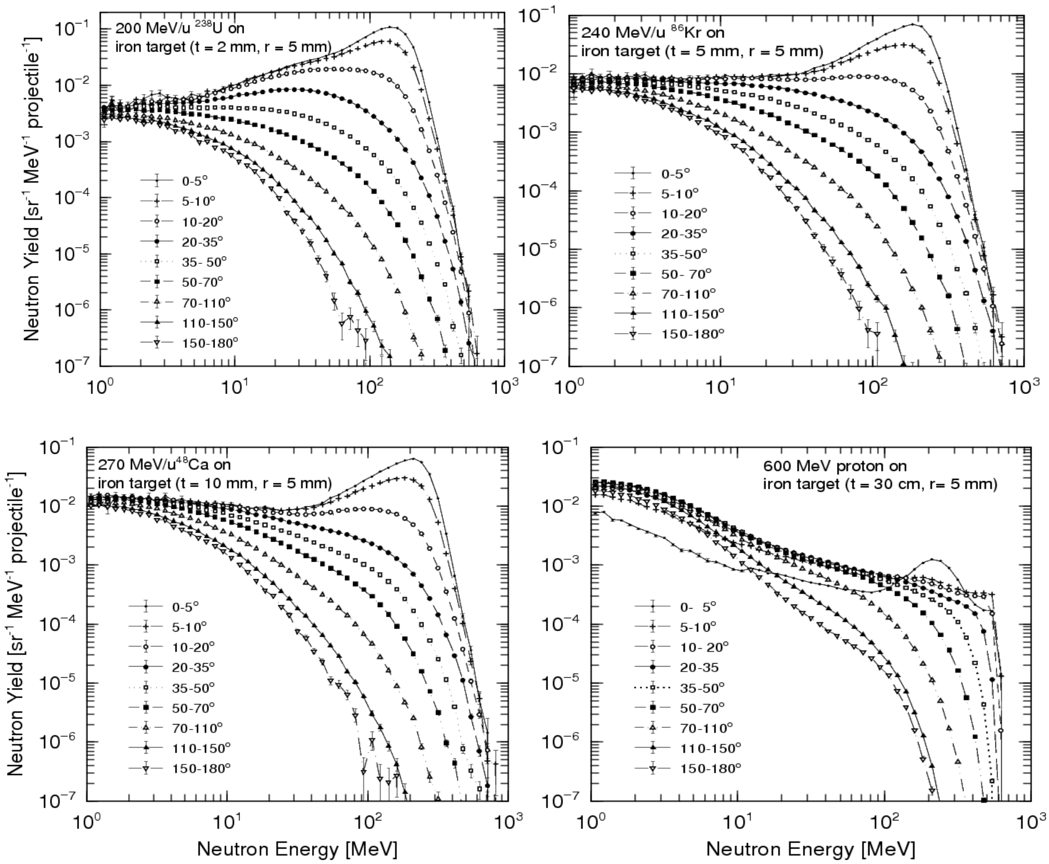

Figure 3: Angular and energy spectra of secondary neutrons from a graphite target

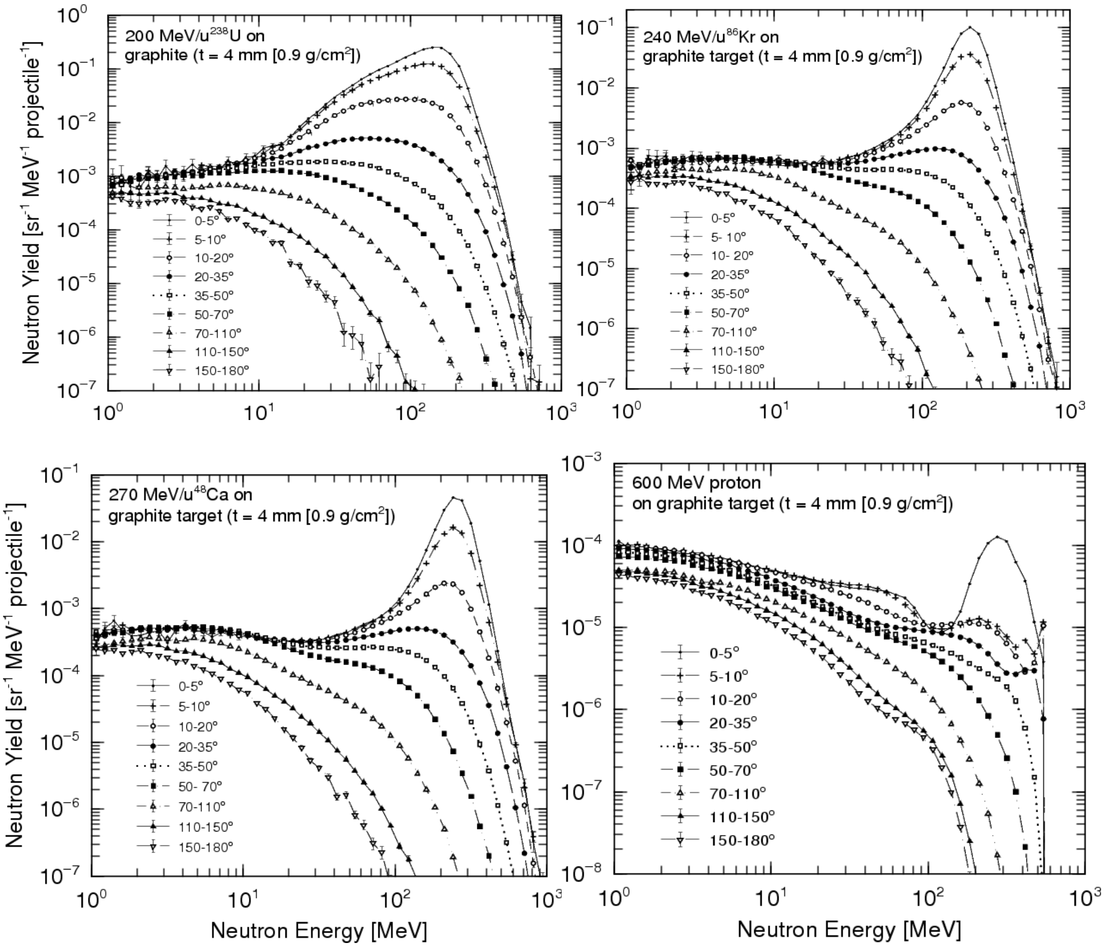

Figure 4: Angular and energy spectra of secondary neutrons from iron and ISOL targets irradiated by 70-MeV protons

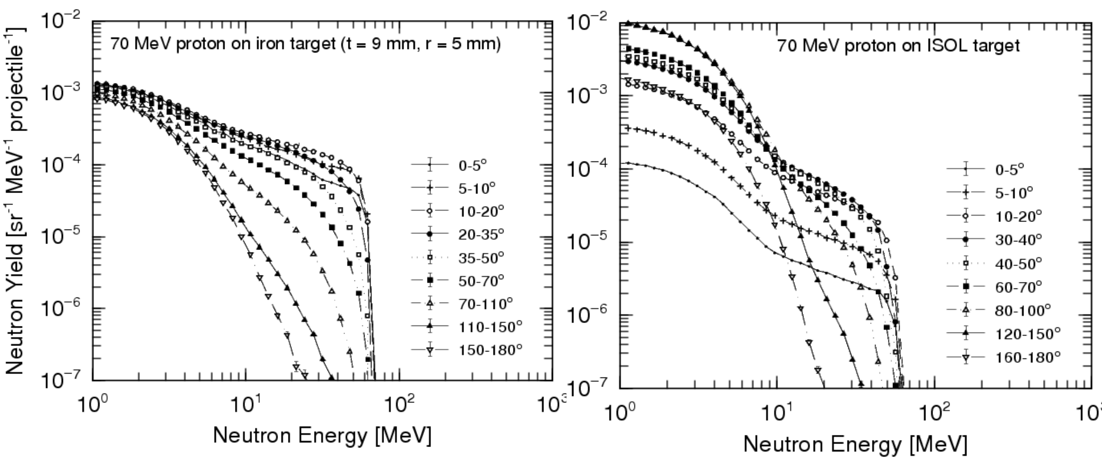

Figures 5(a) and 5(b) show the angular fluxes of high-energy neutrons for the iron and graphite targets, respectively, normalised for a 1-W beam power and integrated above 20 MeV. These figures show that secondary neutrons produced by heavy-ion bombardments have a high degree of forwardness compared with those produced by proton bombardment. For the same beam power, the impact of 600-MeV protons on both targets produced higher fluxes in the sideways and backward directions in comparison with those produced by impact of heavy ions.

Figure 5: Angular flux of high-energy neutrons above 20 MeV for various projectile-target combinations normalised for a 1-W beam injection

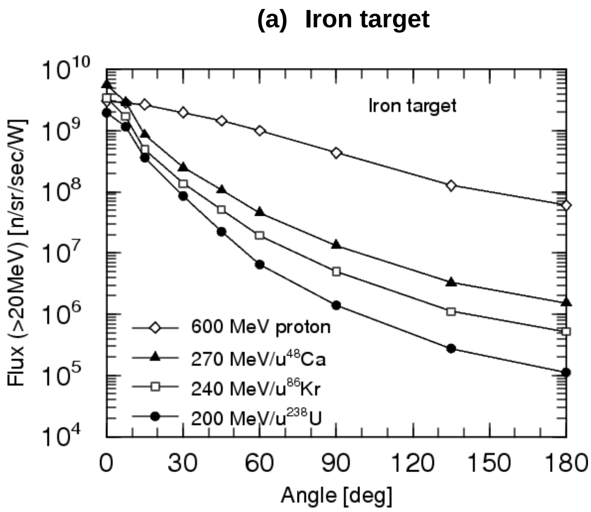

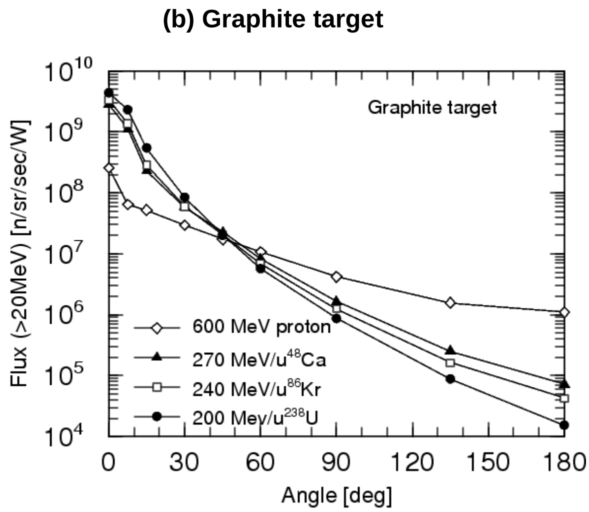

Simulation of neutron attenuation by a massive shield

Having derived the energy spectra of the secondary neutrons, we performed simulations of the transmission of high-energy neutrons above 20 MeV through an 8-m-thick shield using the PHITS Monte Carlo code. A total of 180 transmission simulations were carried out for two targets, five projectiles, nine angles, and two shielding materials. We simulated the injection of a pencil beam of neutrons into the center of the shield slab, and we used an importance method as a variance-reduction technique in the Monte Carlo simulation to obtain good statistics for neutrons in the deep-shielding region. Figure 6 shows two-dimensional neutron-track plots of the shielding transmission simulations with 8-m-thick shields of concrete or iron with neutrons emitted at 0° from an iron target irradiated by a 200-MeV/u ^{238}U beam as an example. The energy spectra of neutrons integrated over planes at the same depth were scored with a surface crossing estimator. Dose rates of high-energy neutrons were estimated from the spectra and from the flux-to-dose conversion factor [7].

Attenuation profiles of the prompt dose rate of high-energy neutrons through the 8-m-thick shields of concrete and iron were obtained for various angles of the neutron sources for all projectile–target combinations. The results for the iron target irradiated by a 200-MeV/u ^{238}U beam are exemplified in Figure 7. As a result of the use of the importance method in the deep-penetration simulation, statistical errors within a few percentage points were obtained, which are sufficiently accurate to permit the estimation of the dose rate through the 8-m thickness. However, the attenuation profiles are strongly dependent on the high-energy part of the source neutron spectra and, because of the strong forwardness of the secondary neutrons emitted as a result of the injection of heavy ions, comparatively poorer statistics are observed in the backward direction, as shown in Figures 2–4. To avoid the risk of underestimating the dose rates, therefore, shielding parameters for 110–150° should be used for the angular direction above 150° for all projectile–target combinations.

Figure 6: Two-dimensional neutron-track plots based on the shielding-transmission simulations using neutrons produced at 0° by irradiation of an iron target by 200-MeV/u ^{238}U

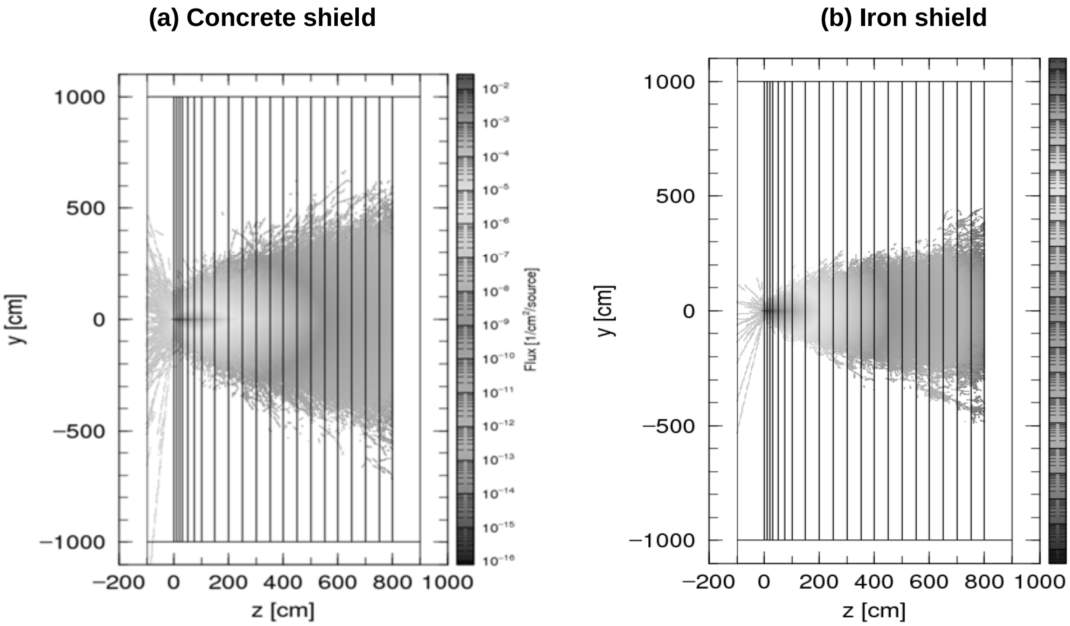

Figure 7: Attenuation profiles of the dose of high-energy neutrons through shields with irradiation of neutron sources at nine different angles from an iron target by 200-MeV/u ^{238}U

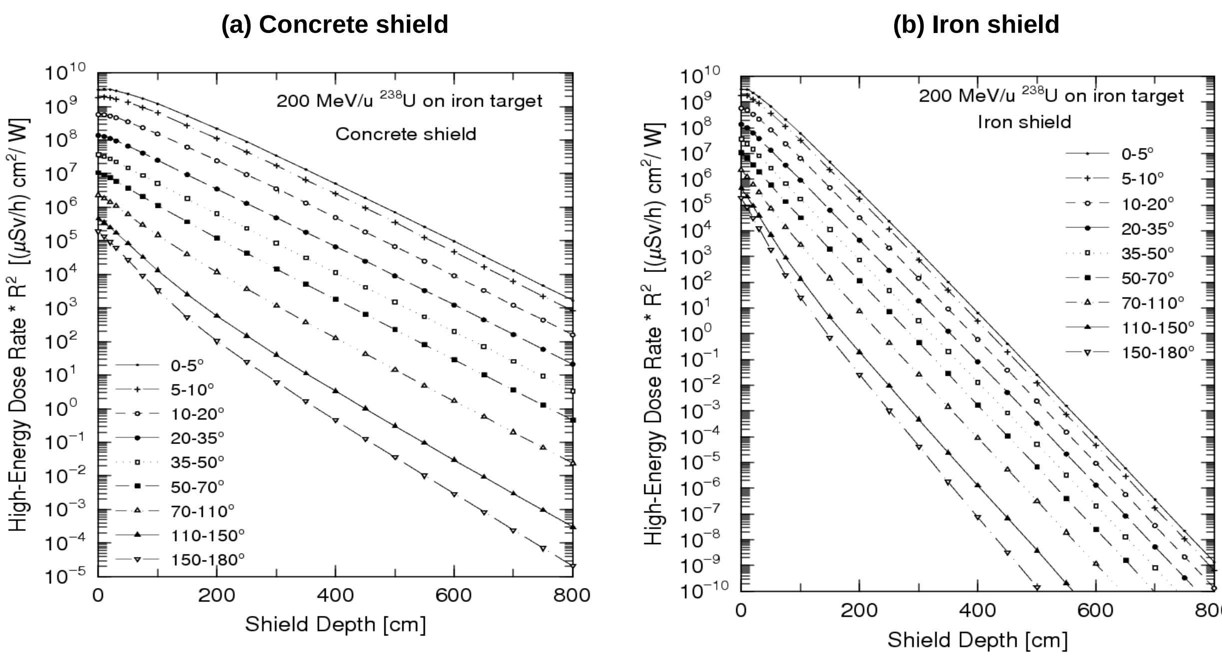

Relationship between the energy spectrum and the dose rate

Concrete shield

A simulation of transmission of neutrons through an 8-m concrete shield in the range of neutron energies down to the thermal level (0.025 eV) was also performed in the case of neutrons generated by irradiation of an iron target by a 200-MeV/u ^{238}U beam. The neutron-energy spectra down to thermal energy levels at various depths in the concrete shield with the neutron source at 0° are shown in Figure 8. Beyond a thickness of about 200 cm in the concrete shield, an equilibrium state is observed in the neutron-energy spectrum down to thermal energy levels; this keeps the shape of the spectrum independent of the shield depth.

Prompt dose rates were estimated for total neutrons, high-energy neutrons above 20 MeV, and photons, using the energy spectra obtained in the simulation described above. Figure 9 shows a comparison of their attenuation profiles. The three attenuation curves in the region beyond a thickness of about 200 cm show an almost constant slope.

Figure 10 shows the ratios of the total dose (including photons and neutrons) over the whole energy range to the dose of high-energy neutrons passing through the concrete shield for various angles. As can be seen in the figure, all ratios become almost constant after a thickness of 250 cm, and the total prompt dose rates are 1.6–1.9 times those of the high-energy neutrons for all angles. Therefore, by taking a correction factor of 2.0 as a safety margin, the total prompt dose rate behind the concrete shield can be predicted from the results for the high-energy neutrons above 20 MeV.

Iron shield

Using the same source neutrons as described above, we also performed a simulation with 6 m iron shield followed by 2 m concrete shield, and we simulated the neutron-energy spectra down to thermal energy levels at various depths in the two layers of the composite iron-and-concrete shield using a weight window method as a variance-reduction technique in the Monte Carlo simulation. The results are shown in Figure 11. An energy spectrum behind an iron shield generally has a broad peak at around a few hundred kiloelectron volts which consists mainly of inelastically scattered neutrons. Where the iron shield is thicker, the contribution of these neutrons increases, whereas that of high-energy neutrons decreases rapidly. However, placing a concrete shield behind the iron shield reduces the flux of neutrons with energies in the region of a few hundred kiloelectron volts and, finally, the energy spectrum settles to an equilibrium state in the concrete shield.

Additional simulations were performed for 1, 2, 4, 6, and 8 m-thick iron shields followed by a massive concrete shield. Dose-attenuation profiles through the shield were estimated for the total neutrons, high-energy neutrons, and photons; these are shown for the cases of the 2 and 4m-thick iron shields in Figure 12, and for the 6 and 8m-thick shields in Figure 13. The figures show that the curves of the total dose rate start to decrease rapidly after the boundary of the concrete shield and that they finally settle into an equilibrium state in which the attenuation curves for the total neutrons and the high-energy neutrons are parallel. These results permitted the dependence of the required thicknesses of the additional concrete on the thickness of the iron shield to be roughly evaluated and the evaluation is presented in Table 2.

As can be seen in Figures 12 and 13, the contribution of photons accompanied by inelastic reactions is not negligible, especially in the case of a thick iron shield. Even behind the required thickness of concrete, dose rates due to photons remain dominant in cases where the thickness of the iron shield is greater than 4m, and the use of an additional shield for photons should be considered in these cases.

Figure 8: Neutron-energy spectra down to thermal energy levels inside a concrete shield for irradiation of a neutron source at 0° from an iron target by 200-MeV/u ^{238}U

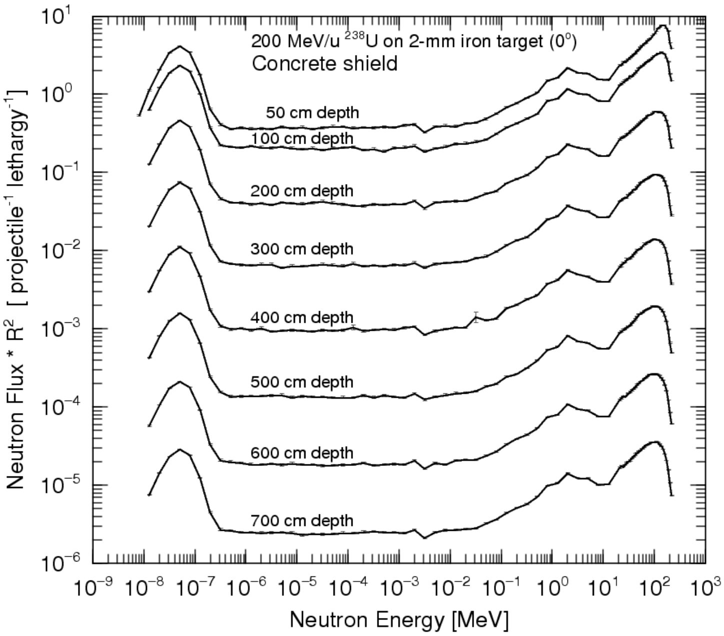

Figure 9: Comparison of attenuation profiles of dose rates of total neutrons, high-energy neutrons above 20 MeV, and photons through a concrete shield for irradiation of neutrons at 0° from an iron target by 200-MeV/u ^{238}U

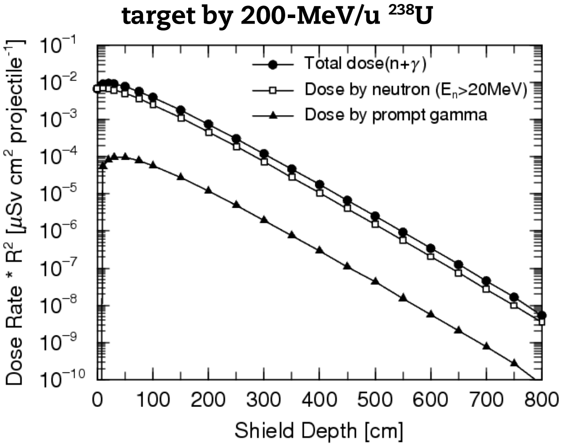

Figure 10: Ratios of total dose to high-energy neutrons through a concrete shield for irradiation of neutrons at various angles from an iron target by 200-MeV/u ^{238}U

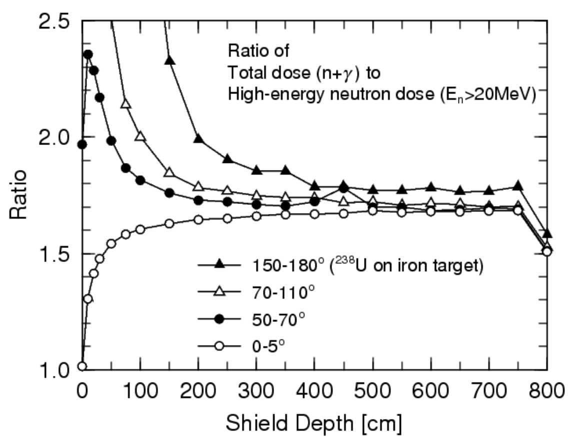

Figure 11: Neutron-energy spectra down to thermal energy levels inside a 6m iron shield followed by a 2 m concrete shield for irradiation of neutrons at 0° from an iron target by 200-MeV/u ^{238}U

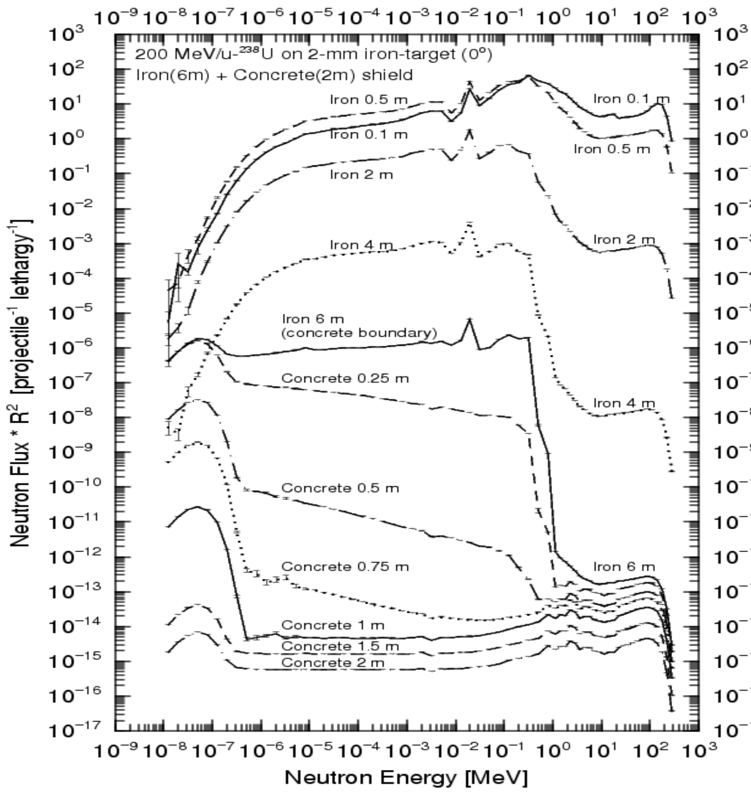

Figure 12: Dose-rate attenuation profiles of total neutrons, high-energy neutrons, and photons inside an iron shield of thickness 2 m (left) or 4 m (right) followed by a thick concrete shield for irradiation of neutrons at 0° from an iron target by 200-MeV/u ^{238}U

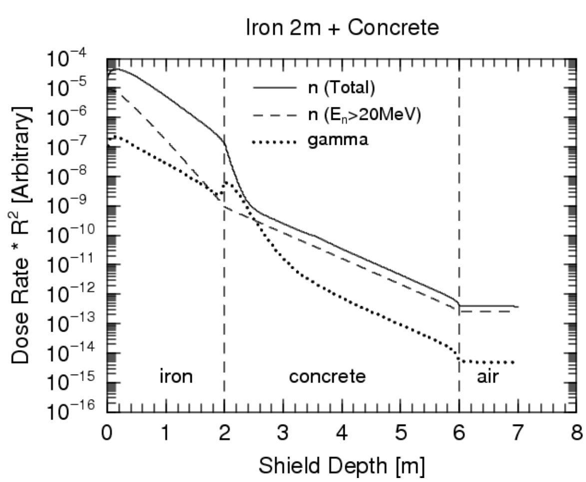

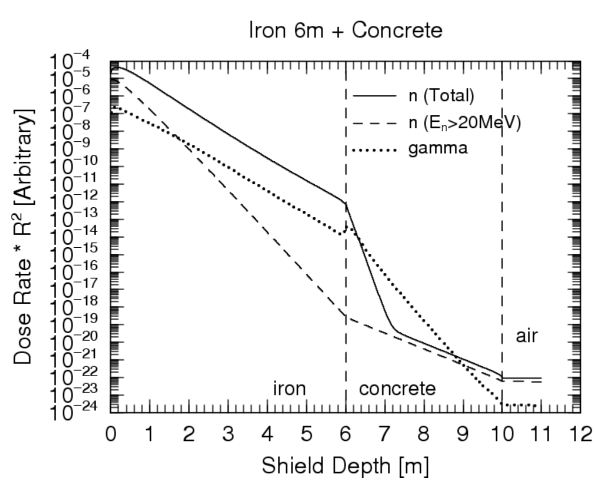

Figure 13: Dose rate attenuation profiles of total neutrons, high-energy neutrons, and photons inside an iron shield of thickness 6 m (left) or 8 m (right) followed by a thick concrete shield for irradiation of neutrons at 0° from an iron target by 200-MeV/u ^{238}U

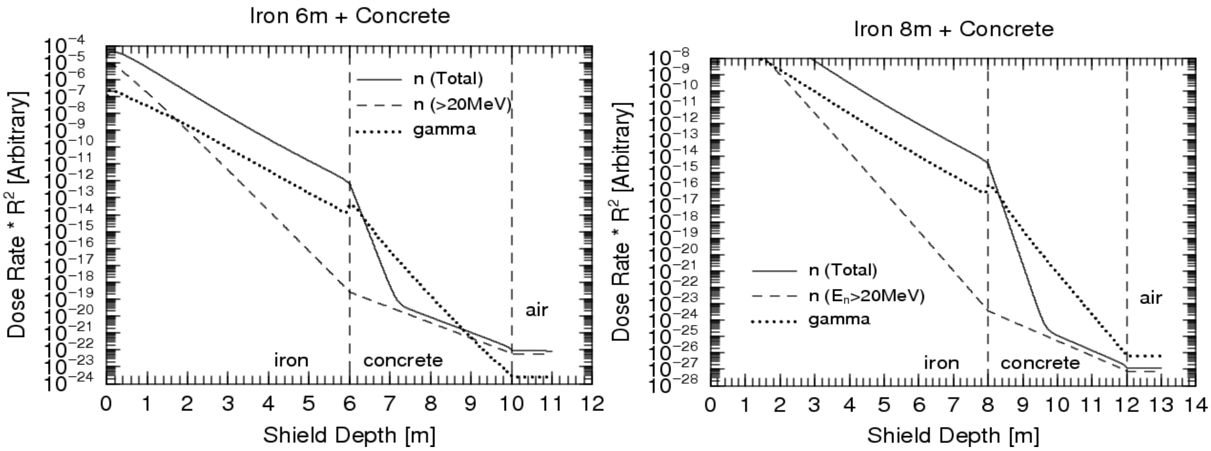

Table 2: Required concrete thickness after various thicknesses of iron shield

Iron thickness	1 m	2 m	4 m	6 m	8 m
Needed last concrete thickness	0.4 m	0.6 m	0.8 m	1.2 m	1.6 m

Simulation of uniform losses

To estimate the shielding parameters for uniform beam loss, Monte Carlo simulations were performed for the iron target with five projectiles and two shielding materials. Instead of placing multiple beam losses uniformly along the beam line, a point loss and long flux estimators that covered most of the transmitted particles in the beam direction were defined to obtain results physically identical to those for uniform loss.

Surface crossing estimators 2 m wide by 110 m long, i.e. from 10 m backward up to 100 m forward, were placed in the various shield thicknesses. Energy spectra of the transmitted neutrons through an 8 m-thick concrete or iron shield in the energy range above 20 MeV were estimated and the dose rates of high-energy neutrons were obtained at various depths in the concrete and iron shields. Figure 14 shows an example of a two-dimensional dose-rate profile obtained by the simulation.

Figure 14: Two-dimensional dose-rate profiles in the three perpendicular planes (*x*=0, *y*=0 and *z*=0) for a uniform-loss equivalent simulation with a 200-MeV/u ^{238}U parallel beam on an iron target

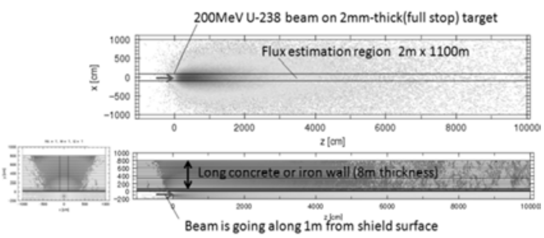

Parameter estimations

The all-attenuation profiles of the prompt dose rates for the point loss that we obtained were fitted using Equation (1) to give the shielding parameters H_0 and λ for high-energy neutrons for various projectile–target combinations and for various angles from the beam direction. The fitting images are exemplified in Figure 15.

The values of H_0 were obtained as values at 0 cm thickness of the shield on the extrapolated fitting lines and, because of a spectrum build-up process, were generally higher for forward angles and lower for backward angles than those for the original data at 0 cm (Figure 15). Finally, the values of H_0 for the high-energy dose were converted into those for the total dose by applying a correction factor of 2.0, as previously discussed.

Two values of H_0 for concrete and iron shields were obtained for one target–projectile combination. Generally, the values for the iron shield were slightly higher than those for the concrete shield because of the steeper slope of the fitted curve in the case of iron. Therefore, the H_0 value for iron was employed for each source term. The maximum difference was less than a factor of two in this work. The shielding parameters that we obtained for point losses are given in Tables 3 and 4 for H_0 and λ, respectively.

The shielding parameters for uniform losses were also estimated by fitting the simulated dose rates with Equation (3). The numerical values of H_0 and λ for five projectiles and two shielding materials are listed in Table 5.

Figure 15: Fitting image for the attenuation profiles of the prompt dose rate in the shield

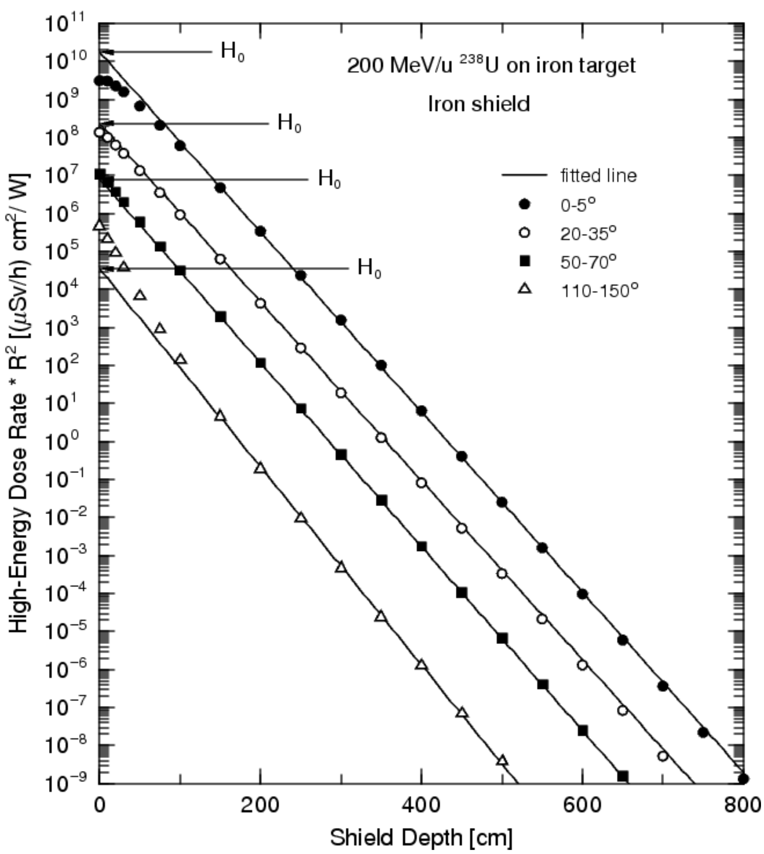

Table 3: Shielding parameter H_0 for various point losses

		H_0[(μSv/h) cm²/W] for point loss							
Target	**Beam**	**0-5°**	**10°**	**20°**	**35°**	**50°**	**70°**	**110°**	**150-180°**
Fe (full stop)	200 MeV/u ^{238}U	3.5E+10	1.8E+10	3.5E+09	4.7E+08	8.7E+07	1.6E+07	1.0E+06	6.9E+04
	240 MeV/u ^{86}Kr	8.1E+10	3.5E+10	6.9E+09	1.0E+09	2.4E+08	5.3E+07	6.1E+06	3.9E+05
	270 MeV/u ^{48}Ca	1.5E+11	6.5E+10	1.3E+10	2.1E+09	5.9E+08	1.4E+08	1.8E+07	1.2E+06
	600 MeV proton	9.7E+10	8.5E+10	6.8E+10	3.8E+10	1.9E+10	7.3E+09	1.4E+09	1.9E+08
	70 MeV proton	1.5E+09	2.6E+09	2.6E+09	1.4E+09	5.4E+08	1.9E+08	2.7E+07	2.2E+06
Graphit (0.9 g/cm² thick)	200 MeV/u ^{238}U	8.3E+10	3.7E+10	6.9E+09	7.8E+08	1.1E+08	1.5E+07	7.3E+05	2.4E+04
	240 MeV/u ^{86}Kr	1.1E+11	4.2E+10	7.7E+09	1.1E+09	2.3E+08	3.6E+07	2.2E+06	5.4E+04
	270 MeV/u ^{48}Ca	1.1E+11	4.0E+10	7.0E+09	1.2E+09	3.0E+08	5.4E+07	3.8E+06	1.3E+05
	600 MeV proton	1.0E+10	1.8E+09	1.6E+09	6.7E+08	2.7E+08	9.0E+07	1.5E+07	3.8E+06
ISOL UC_2	70 MeV proton	5.4E+07	1.9E+08	6.0E+08	5.6E+08	3.3E+08	1.5E+08	6.3E+07	1.2E+07

∗ Interpolation is recommended for angles where parameters are not given.

Table 4: Shielding parameter λ for various point losses

		λ[g/cm²] for point loss							
Shield	**Beam**	**0-5°**	**10°**	**20°**	**35°**	**50°**	**70°**	**110°**	**150-180°**
Concrete	200 MeV/u ^{238}U	117	117	117	116	114	111	106	96
	240 MeV/u ^{86}Kr	124	123	123	122	119	114	108	101
	270 MeV/u ^{48}Ca	126	126	125	124	120	116	110	102
	600 MeV proton	128	129	128	127	124	119	112	105
	70 MeV proton	63	62	61	60	58	58	54	54
Iron	200 MeV/u ^{238}U	143	143	144	144	142	140	139	130
	240 MeV/u ^{86}Kr	147	147	147	147	145	143	138	134
	270 MeV/u ^{48}Ca	149	149	148	148	146	143	139	135
	600 MeV proton	150	150	150	150	149	145	140	135
	70 MeV proton	88	88	87	85	83	82	79	78

∗ Interpolation is recommended for angles where parameters are not given.

Table 5: Shielding parameters H_0 and λ for various uniform losses

Target	Beam	Concrete shield		Iron shield	
		H_o[(μSv/h) cm/(W/m)]	λ[g/cm^2]	H_o[(μSv/h) cm/(W/m)]	λ[g/cm^2]
Fe (full stop)	200 MeV/u ^{238}U	3.0E+05	97	1.3E+05	134
	240 MeV/u ^{86}Kr	7.5E+05	99	3.6E+05	136
	270 MeV/u ^{48}Ca	1.6E+06	101	6.8E+05	135
	600 MeV proton	3.4E+07	105	3.7E+07	138
	70 MeV proton	7.3E+05	56	2.8E+05	84

Comparisons of dose-rate results calculated by formula and by simulation

For a simple shielding structure, dose rates calculated by means of the empirical formula were compared with those obtained by simulation with the PHITS code in the case of a distance of 1 m between the target and the shield. A two-dimensional track plot obtained by simulation with a ^{238}U parallel beam is shown in Figure 16. The simulated dose-rate distributions at several depths as a function of the angle for a 600-MeV proton beam and a 200-MeV/u ^{238}U beam are shown in Figure 17, together with the results calculated using Equation (1) with the appropriate parameters.

In the case of the proton beam shown in the figure, the results calculated using the formula agreed well with those obtained by simulation. However, in the case of the ^{238}U beam, the formula sometimes underestimated the results in thick regions at forward angles because of the strong forwardness of neutrons. Therefore, for heavy-ion injection of a parallel beam, the formula can be applied at angles of more than 80° for thicknesses of concrete in excess of 3 m.

Figure 16: Two-dimensional track plots of neutrons with an 8-m concrete shield for a 2 mm-thick iron target irradiated with a 200-MeV/u ^{238}U beam in the direction parallel to the shield surface

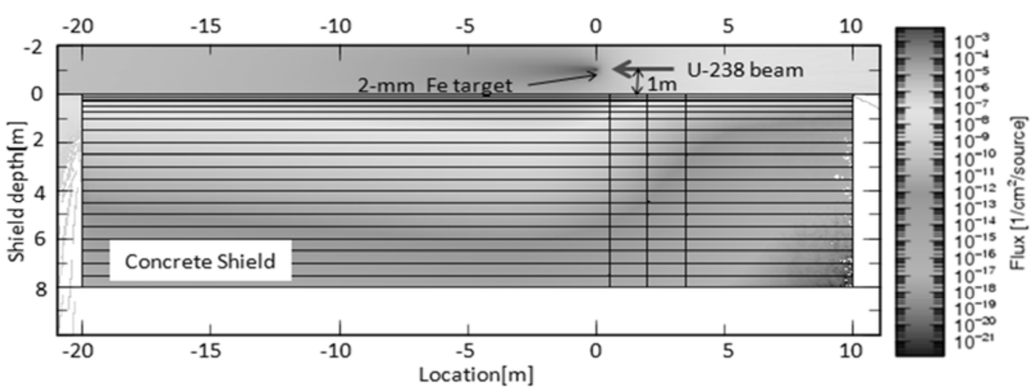

Figure 17: Comparisons of dose-rate distributions obtained by PHITS simulations and by calculations using the formula along the angles from the beam direction at the same shield depth inside an 8 m concrete shield for an iron target irradiated with a 600-MeV proton beam (left) or with a 200-MeV/u ^{238}U beam (right) in the direction parallel to the shield surface

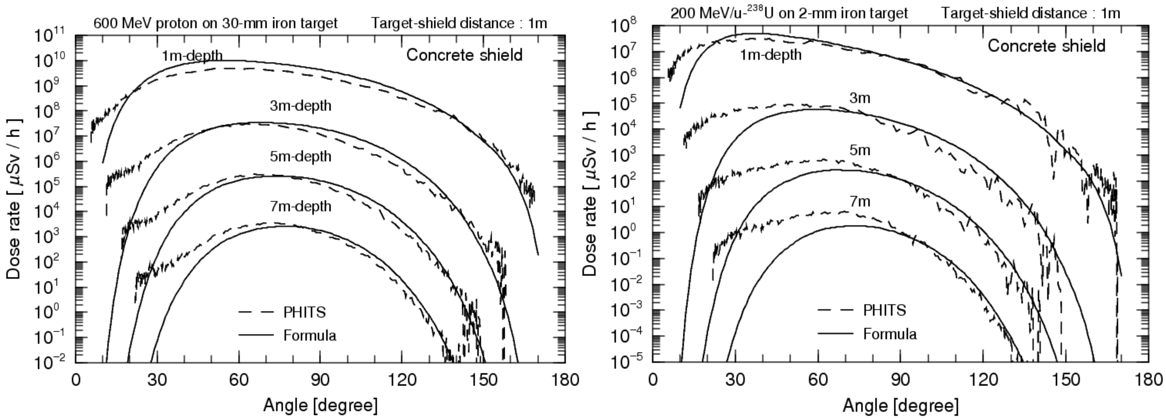

A two-dimensional track plot for the perpendicular beam is shown in Figure 18. The results obtained by simulation and those obtained by the formula, compared as a function of the angle from 0° to 70°, are shown in Figure 19.

For the case of the ^{238}U beam, in the angular range below 10°, the formula gives dose rates that are higher by about a factor of 2 than those given by the simulation. Apart from this, however, the dose rates calculated using the formula generally agreed with those given by simulation over the angular range between 0 and 60° for concrete shields with a thickness of more than 3 m for both the proton beam and the ^{238}U beam.

Figure 18: Two-dimensional track plot of neutrons with an 8-m concrete shield for a 2 mm-thick iron target irradiated by a 200-MeV/u ^{238}U beam in the direction perpendicular to the shield surface

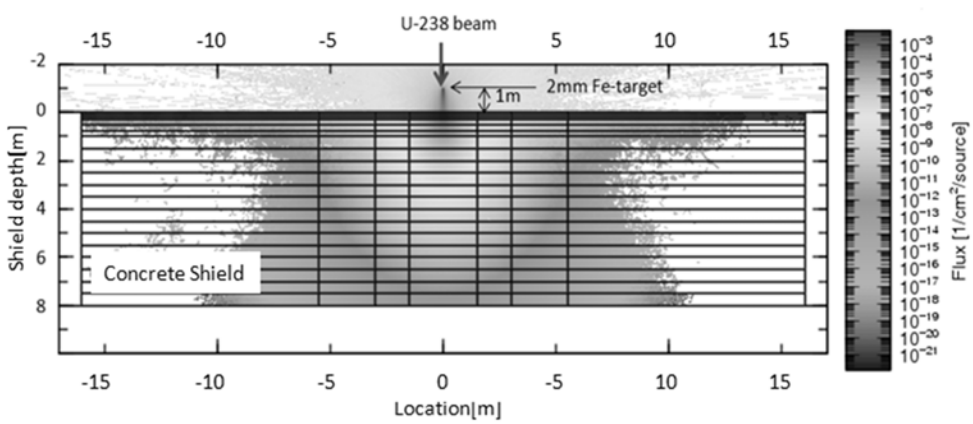

Figure 19: Comparisons of dose rate distributions obtained by PHITS simulation and by calculation with the formula along the angles from the beam direction at the same shield depth inside an 8-m concrete shield for an iron target irradiated with a 600-MeV proton beam (left) or with a 200-MeV/u ^{238}U beam (right) in the direction perpendicular to the shield surface

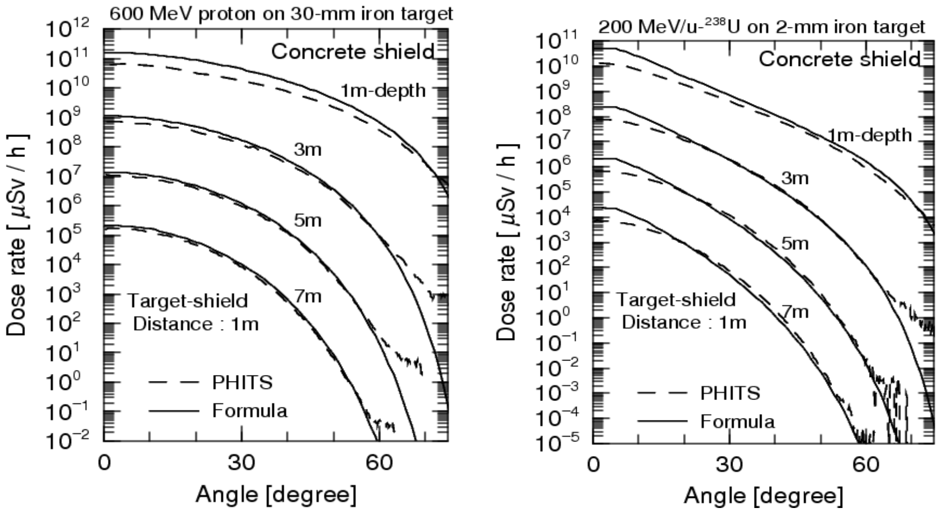

Conditions and limitations for practical application of the formula

The parameters of the empirical formulae obtained in this work are applicable under the following conditions and with the following limitations.

- The total of the thickness of the concrete shield plus 2.5-times the thickness of the iron shield should be at least 250 cm.

The fitting regions for the attenuation profiles have thicknesses of between 250 and 700 cm for concrete and between 100 and 600 cm for iron; therefore, these parameters should be used for dose estimation points in the region where the thicknesses of the shields are greater than 250 cm for concrete and 100 cm for iron. Because the shielding ability of iron is about 2.5 times greater than that of concrete, the sum of the thickness of the concrete and 2.5 times the thickness of the iron should exceed 250 cm for a multilayer shield.

- An appropriate thickness of concrete should be used for the final shield.

The shielding parameters were estimated on the assumption that the neutron-energy spectrum is in an equilibrium state behind a concrete shield. For the case of a thick iron shield, the required thicknesses of the additional concrete shields are given in Table 2.

- For the point-loss case, the angle to the estimation point should be within the ranges 0–60° for a perpendicular beam, 60-150° for a parallel proton beam, and 80-150° for a parallel heavy-ion beam.

As shown in Figure 20, as the angle from the perpendicular line increases, the portion of the shield in the direct path becomes much longer, so that neutrons passing through the other, shorter, path sometimes contribute markedly (the short-path effect) under actual conditions. Because of the strong forwardness of secondary particles produced by heavy-ion interactions, the short path effect of particles at a small (forward) angle is significant for parallel beams of heavy ions, and the empirical formula gives underestimations in the angular range below 80°. On the other hand, for a perpendicular heavy-ion beam, the short path effect is negligible and the formula applies at comparatively wide angles of up to 60°.

Figure 20: Image showing the direct path and a shorter path to the estimation point

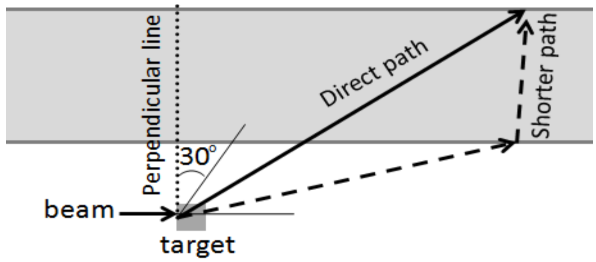

Summary

Shielding parameters for use in an empirical formula for designing shields in a heavy-ion facility were estimated by means of a PHITS Monte Carlo simulation, and the source term and the attenuation length were summarised for various projectiles, targets, angles, and shielding materials. Conditions where the formula applies in terms of the minimum shield thickness, the presence of a final concrete shield, and angular limitations were clarified. The shielding parameters obtained in this work could be very useful in the conceptual design of massive shields for high-power heavy-iron accelerator facilities.

Acknowledgements

The authors thank Dr. Hiroshi Iwase (KEK) and Dr. Koji Niita (RIST) for their useful advice regarding the PHITS Monte Carlo code.

References

[1] B.J. Moyer (1962), *Proc. 1st Int. Conf. Shielding around High Energy Accelerators*, Presses Universitaires de France: Paris, p 65.

[2] S. Ban *et al.* (1980), "Measurement of Transverse Attenuation Length for Paraffin, Heavy Concrete and Iron Around an External Target for 12 GeV Protons", *Nucl. Instrum. Methods* 174, 271.

[3] G.R. Stevenson *et al.* (1982), "Determination of Transverse Shielding for Proton Accelerators Using the Moyer Model", *Health Phys.* 43, 13.

[4] K. Niita *et al.* (2010), "PHITS: Particle and Heavy Ion Transport Code System, Version 2.23", *JAEA-Data/Code 2010-022*.

[5] K. Shibata *et al.* (2002), "Japanese Evaluated Nuclear Data Library Version 3 Revision-3: JENDL-3.3," J. Nucl. Sci. Technol. 39*, 1125*.

[6] H.G. Hughes *et al.* (1996), "Information on the Photon Library MCPLIB02," *Los Alamos National Laboratory Internal Memorandum, X-6: HGH-93-77* and *LA-UR-98-539*.

[7] A. Ferrari *et al.* (1996), "Fluence to Effective Dose and Effective Dose Equivalent Conversion Coefficients for Photons from 50 keV to 10 GeV", *Radiat. Prot. Dosim.* 67, 245.